Supplementary Information

Equal resistance single and bilayer films decouple role of solid electrolyte interphase from lithium morphology in batteries

Sanzeeda Baig Shuchi[1†], Kenzie M. Sanroman Gutierrez[1†], Alexander B. Shearer[1], Solomon T. Oyakhire[1], Yi Cui[2,3,4], Stacey F. Bent[1,3]

[1]Department of Chemical Engineering, Stanford University, Stanford, California 94305, USA.

[2]Department of Materials Science and Engineering, Stanford University, Stanford, California 94305, USA.

[3]Department of Energy Science and Engineering, Stanford University, Stanford, California 94305, USA.

[4]Stanford Institute for Materials and Energy Sciences, SLAC National Accelerator Laboratory, 2575 Sand Hill Road, Menlo Park, California 94025, USA.

† These authors contributed equally.

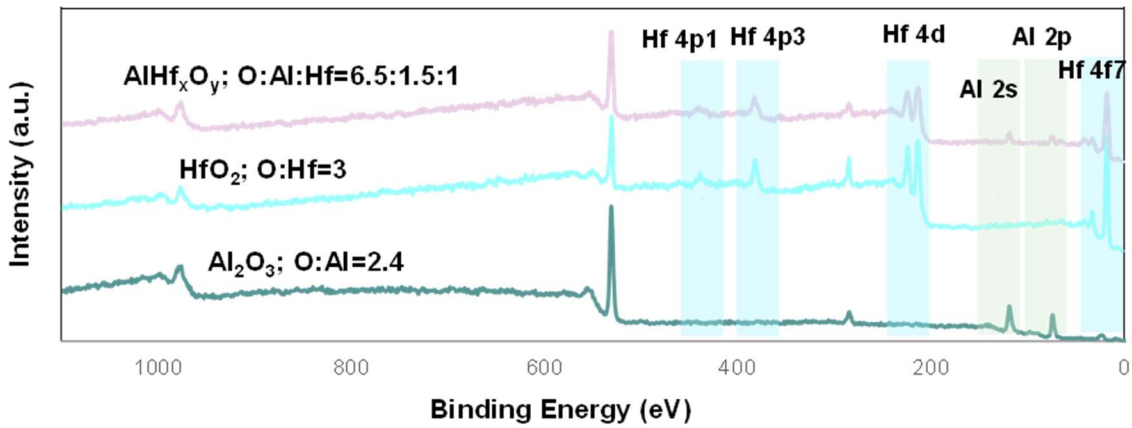

Supplementary Fig. 1. XPS survey scans of as-deposited MO_x thin films on Cu substrates (from bottom to top): 8 nm Al_2O_3-Cu, 13 nm HfO_2-Cu, and 10 nm $AlHf_xO_y$-Cu. Oxygen-to-metal ratios of the thin films are noted in the figure.

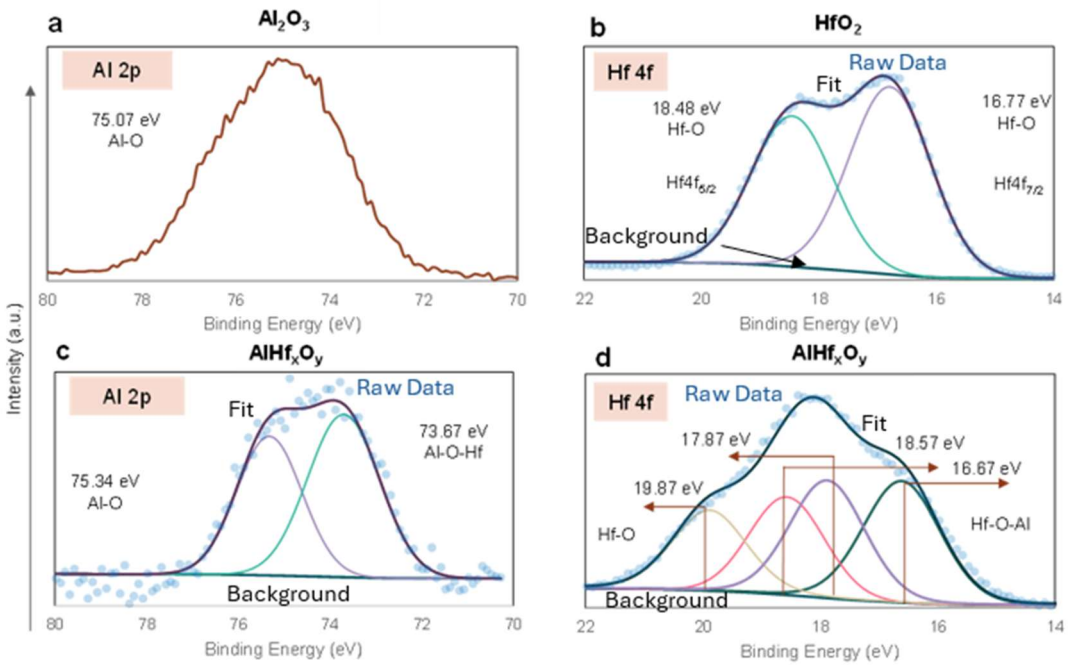

Supplementary Fig. 2. XPS HR scans of corresponding metal peaks of as-deposited MO_x thin films on Cu substrates. a. Al 2p region of 8 nm Al_2O_3-Cu. b. Hf 4f region of 13 nm HfO_2-Cu. c. Al 2p region of 10 nm $AlHf_xO_y$-Cu. d. Hf 4f region of 10 nm $AlHf_xO_y$-Cu.

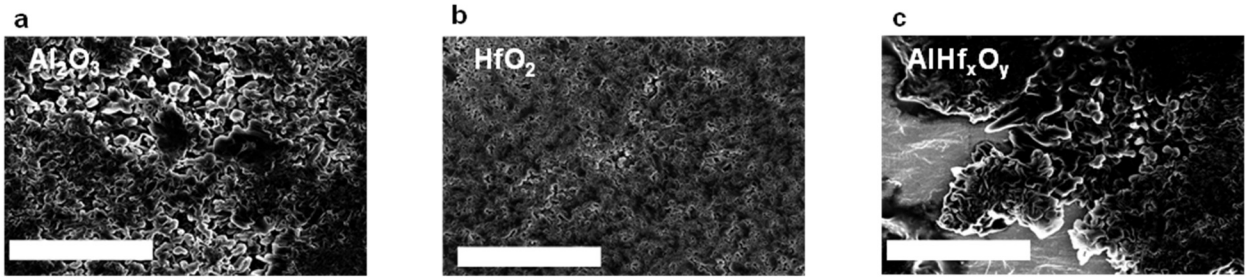

Supplementary Fig. 3. Magnified version of lithium morphology on a. 8 nm Al_2O_3-, b. 13 nm HfO_2-, and c. 10 nm $AlHf_xO_y$-modified Cu current collector after 1st cycle lithium plating using 1 M $LiPF_6$/EC-DEC electrolyte at 1 mA cm^{-2} current density and 0.5 mAh cm^{-2} capacity. The scale bar is 30 µm wide.

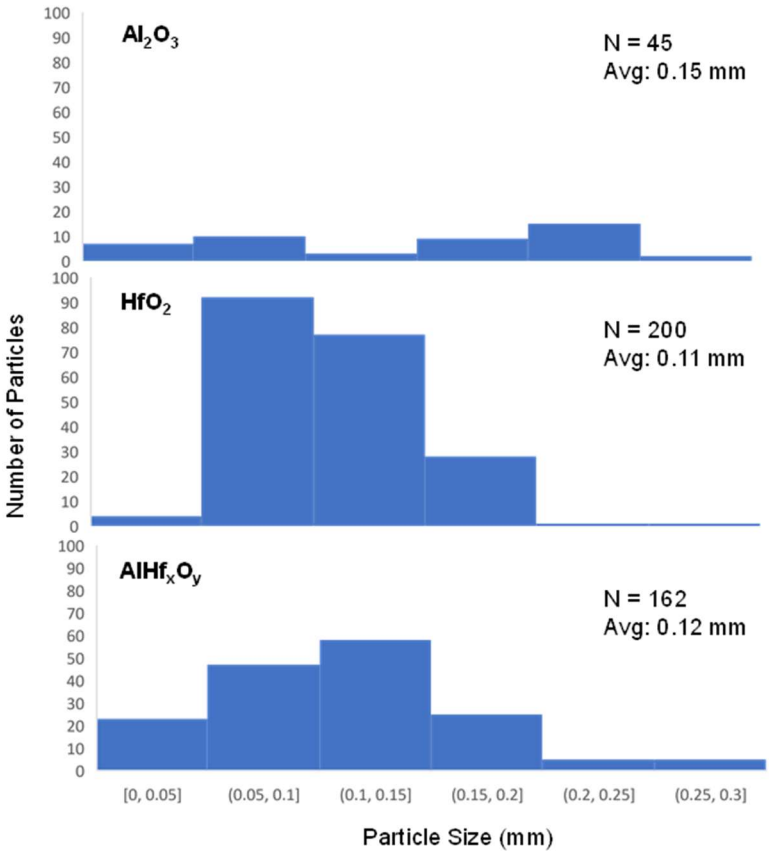

Supplementary Fig. 4. Particle size distribution of electrodeposited Li at 0.5 mAh cm^{-2} and 1 mA cm^{-2} on different fixed resistance thin film-modified Cu substrates with 1 M $LiPF_6$/EC-DEC electrolyte: 8 nm Al_2O_3-, 13 nm HfO_2-, and 10 nm $AlHf_xO_y$-modified Cu (from top to bottom).

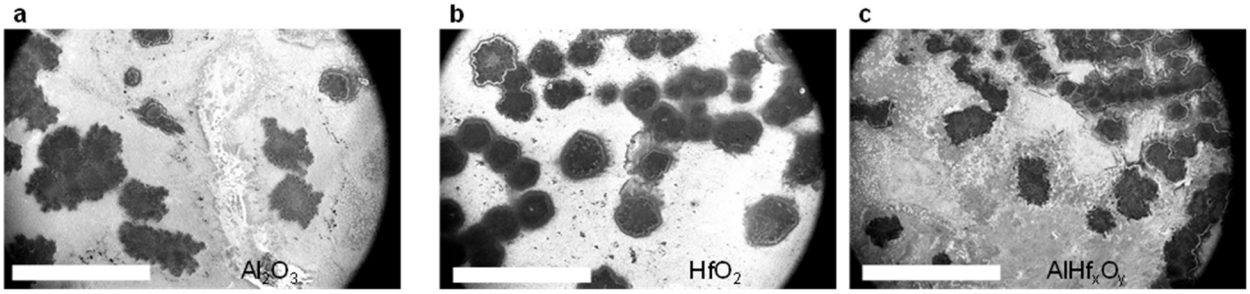

Supplementary Fig. 5. Lithium morphology on a. 8 nm Al_2O_3-, b. 13 nm HfO_2-, and c. 10 nm $AlHf_xO_y$-modified Cu current collector after 1st cycle lithium plating using 1 M $LiPF_6$/EC-DEC electrolyte at 1 mA cm^{-2} current density and 0.25 mAh cm^{-2} capacity. The scale bar is 1 mm wide.

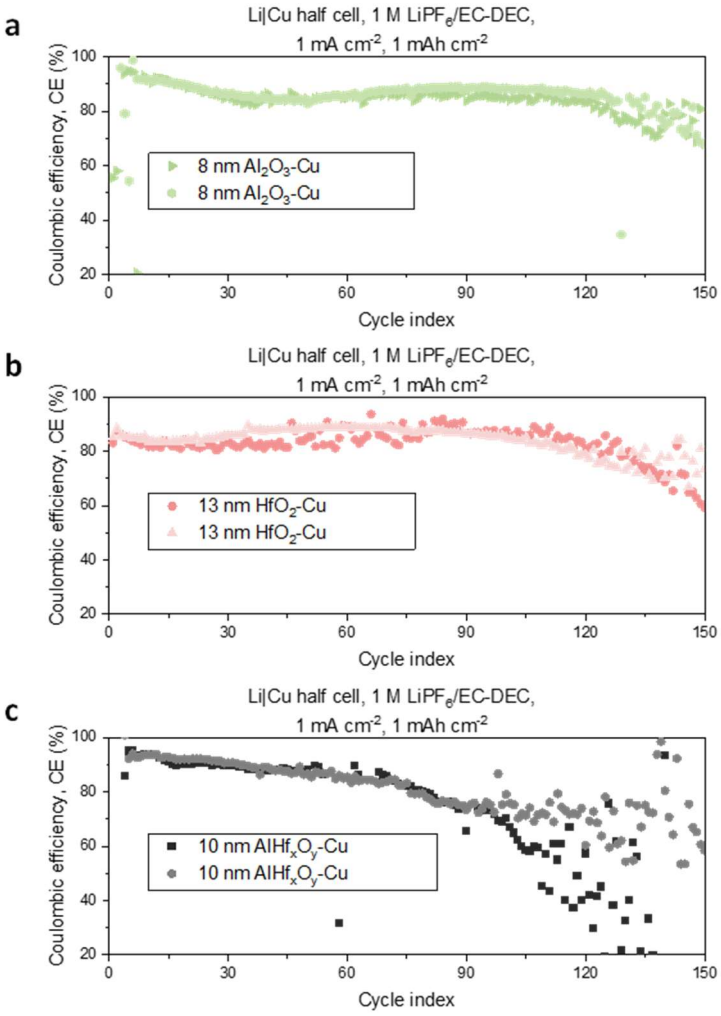

Supplementary Fig. 6. Replicates of long-term cycling performance with a. 8 nm Al_2O_3-Cu, b. 13 nm HfO_2-Cu, and c. 10 nm $AlHf_xO_y$-Cu. Experiments are performed in Li|Cu half-cells using 1 M $LiPF_6$/EC-DEC electrolyte at 1 mA cm^{-2} current density and 1 mAh cm^{-2} plating capacity.

Supplementary Table 1. LiF/C values from peak areas in Fig. 3c and Fig. 3d.

Substrate	XPS analysis region	F/C	Percentage of LiF in F 1s peak (%)	LiF/C
Al_2O_3-Cu	Fig. 3c	2.17	7	0.15
$AlHf_xO_y$-Cu	Fig. 3d	0.46	22	0.10

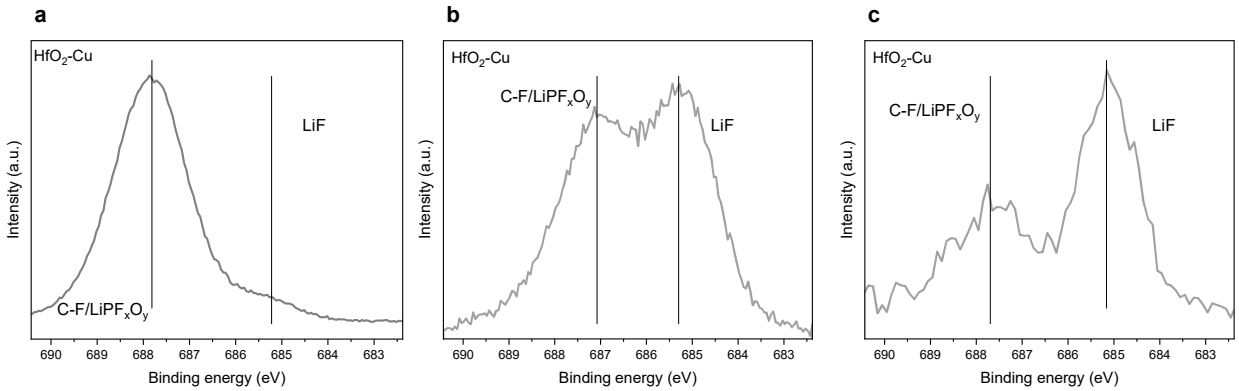

Supplementary Fig. 7. XPS high-resolution scans of F 1s peak regions of SEIs formed on 13 nm HfO_2-Cu with a. Protocol i) SEI prior to the onset of nucleation with potential hold above Li electrodeposition potential, 10 mV vs. Li/Li^+ for 3 hr. b. Protocol ii) SEI after first cycle plating of 0.5 mAh cm^{-2} Li at a current density 1 mA cm^{-2}. c. Protocol iii) SEI atop Li after first plating of 2 mAh cm^{-2} Li at a current density 1 mA cm^{-2}.

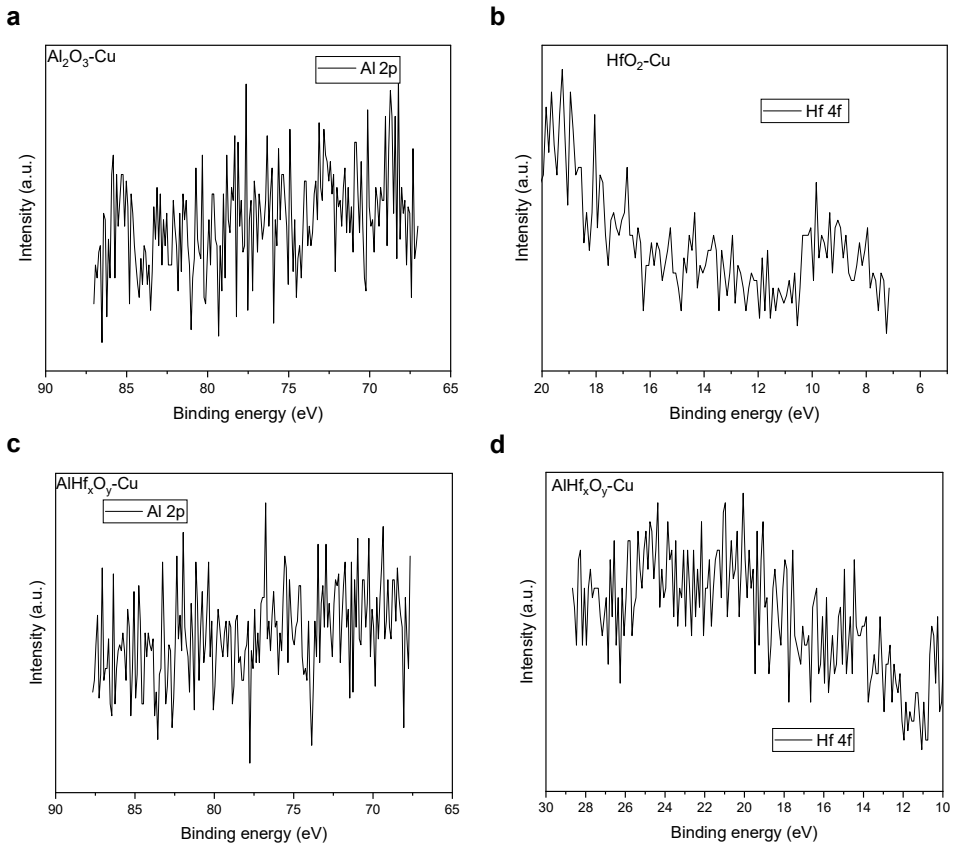

Supplementary Fig. 8. XPS high-resolution scans of metal peak regions during SEI characterization atop Li. for a. Al 2p region of 8 nm Al_2O_3-Cu,b. Hf 4f region of 13 nm HfO_2-Cu, c. Al 2p region of 10 nm $AlHf_xO_y$-Cu, and d. Hf 4f region of 10 nm $AlHf_xO_y$-Cu.

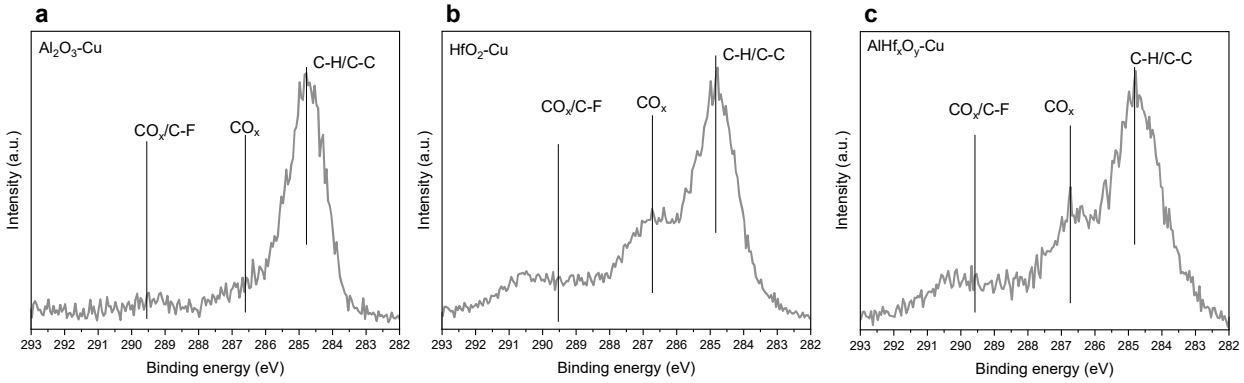

Supplementary Fig. 9. XPS high-resolution scans of C 1s peak regions of SEIs formed on a. 8 nm Al_2O_3-Cu, b. 13 nm HfO_2-Cu, and c. 10 nm $AlHf_xO_y$-Cu with protocol ii) after first cycle plating of 0.5 mAh cm^{-2} Li at a current density 1 mA cm^{-2}.

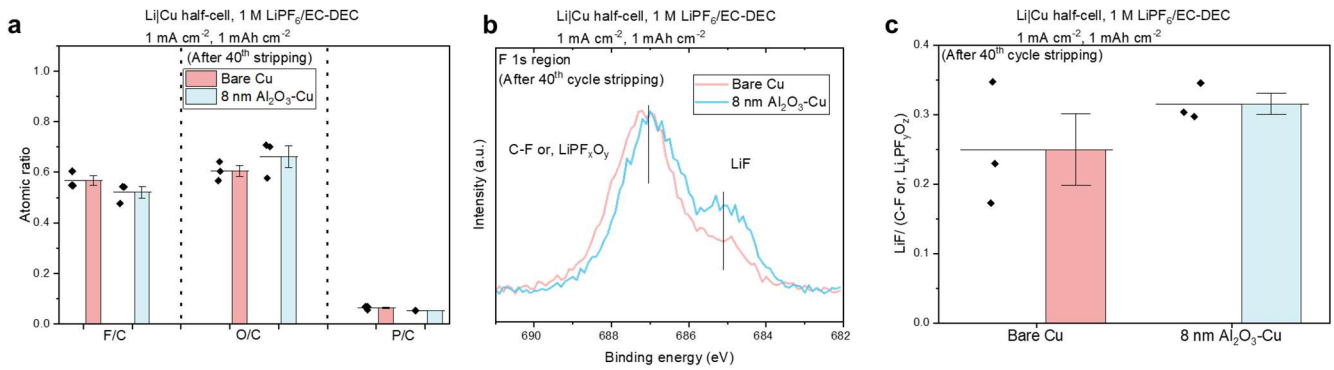

Supplementary Fig. 10. Residual SEI chemical composition analysis using XPS to probe anion-derived nature (atomic ratios), and stability (relative LiF amount) of SEI after 40th cycle stripping. a. The F/C, O/C and P/C atomic ratios; b. the F 1s high resolution (HR) scan; and c. relative LiF amount for the 8 nm Al_2O_3-Cu and bare Cu sample.

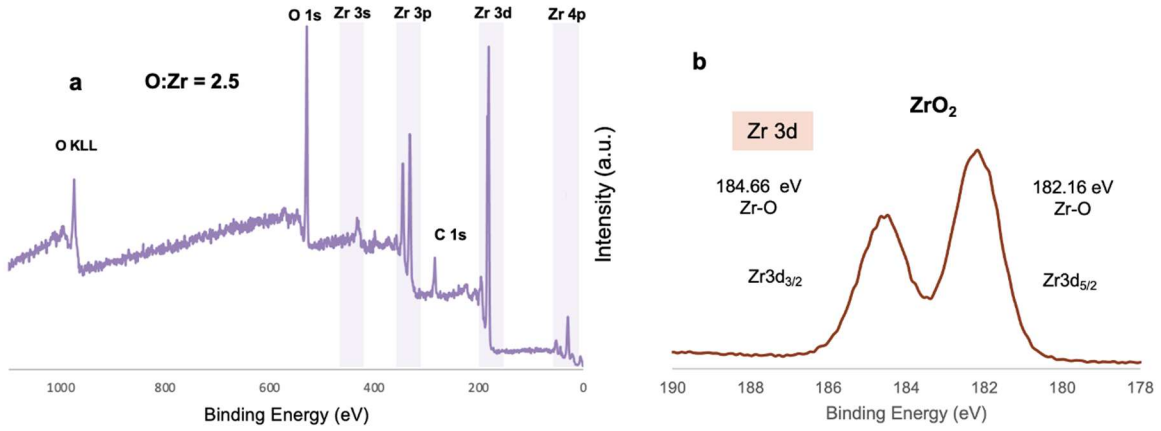

Supplementary Fig. 11. a. XPS survey scan and b. HR scan for Zr 3d region of 17 nm ZrO_2 as deposited onto a Cu substrate.

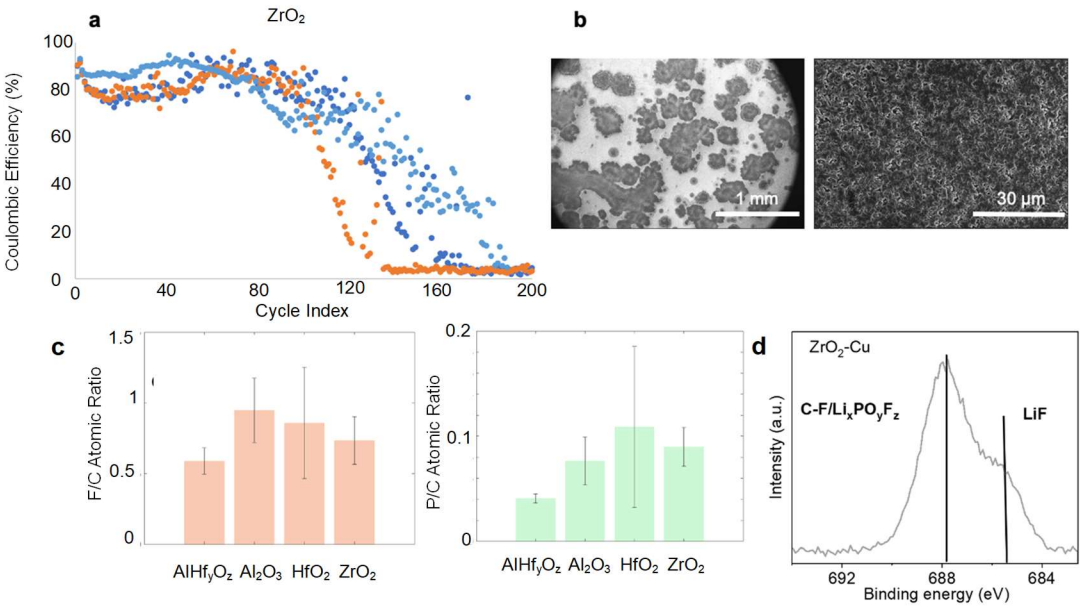

Supplementary Fig. 12. Compiled data for ZrO_2-modified Cu. a. Long -term cycling performance with 17 nm ZrO_2-modified Cu. Experiments are performed in Li|Cu half-cells at 1 mA cm^{-2} current density and 1 mAh cm^{-2} plating capacity. b. Lithium morphology on 17 nm ZrO_2-modified Cu current collector after 1st cycle lithium plating at 1 mA cm^{-2} current density and 0.5 mAh cm^{-2} capacity. c. Atomic ratios for F/C and P/C acquired using XPS for Li|Cu half cells modified with $AlHf_xO_y$, Al_2O_3, HfO_2, and ZrO_2 held at 1 mA cm^{-2}, 0.5 mAh cm^{-2}, where n = 3 and error bars represent one standard deviation. d. HR F 1s peaks acquired using XPS for Li|Cu half cells modified with ZrO_2 using 1 mA cm^{-2} current density and 0.5 mAh cm^{-2} plating capacity. All experiments used 1 M $LiPF_6$/EC-DEC electrolyte.

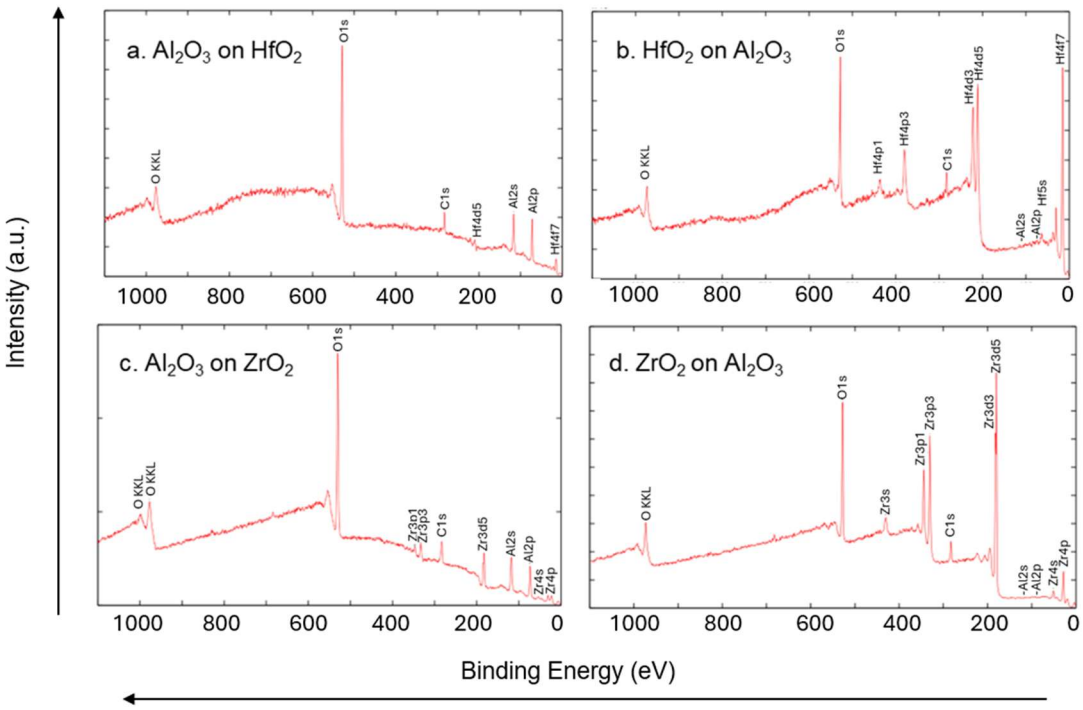

Supplementary Fig. 13. XPS survey scans of as-deposited a. Al_2O_3 on HfO_2-Cu, b. HfO_2 on Al_2O_3-Cu, c. Al_2O_3 on ZrO_2-Cu, and d. ZrO_2 on Al_2O_3-Cu.

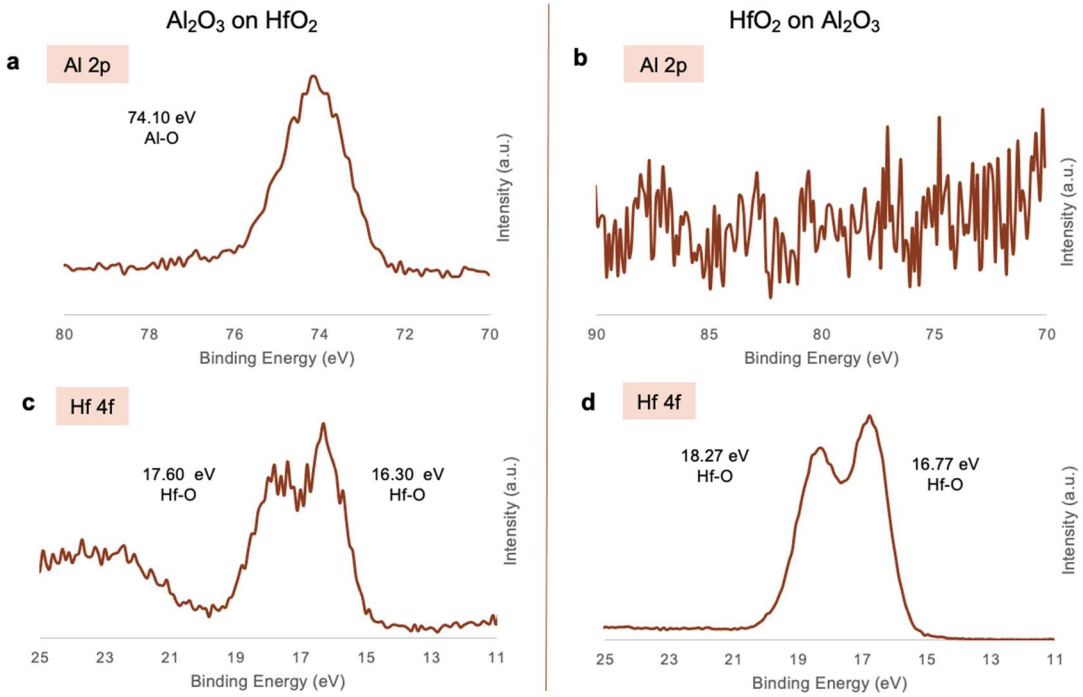

Supplementary Fig. 14. XPS HR scans of the a. Al 2p region for Al_2O_3 on HfO_2-Cu, b. Al 2p region for HfO_2 on Al_2O_3-Cu, c. Hf 4f region for Al_2O_3 on HfO_2-Cu, and d. Hf 4f region for HfO_2 on Al_2O_3-Cu.

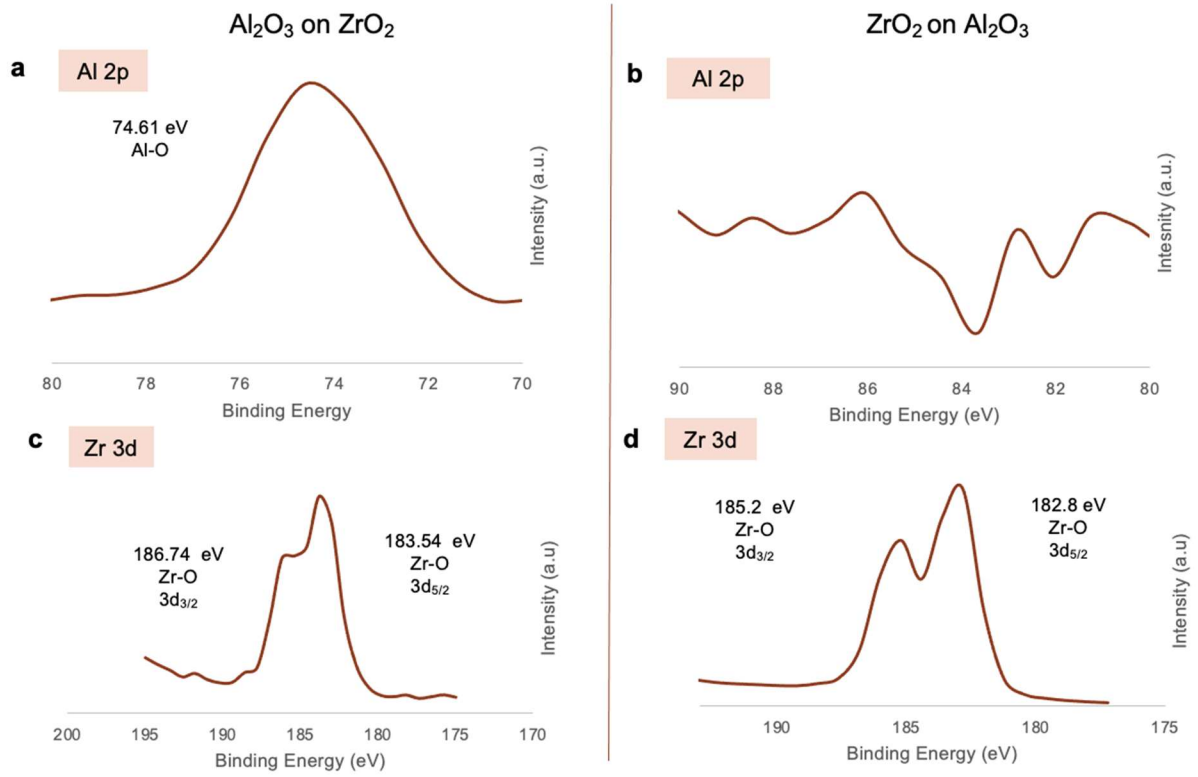

Supplementary Fig. 15. XPS HR scans of the a. Al 2p region for Al_2O_3 on ZrO_2-Cu, b. Al 2p region for ZrO_2 on Al_2O_3-Cu, c. Zr 3d region for Al_2O_3 on ZrO_2-Cu, and d. Zr 3d region for ZrO_2 on Al_2O_3-Cu.

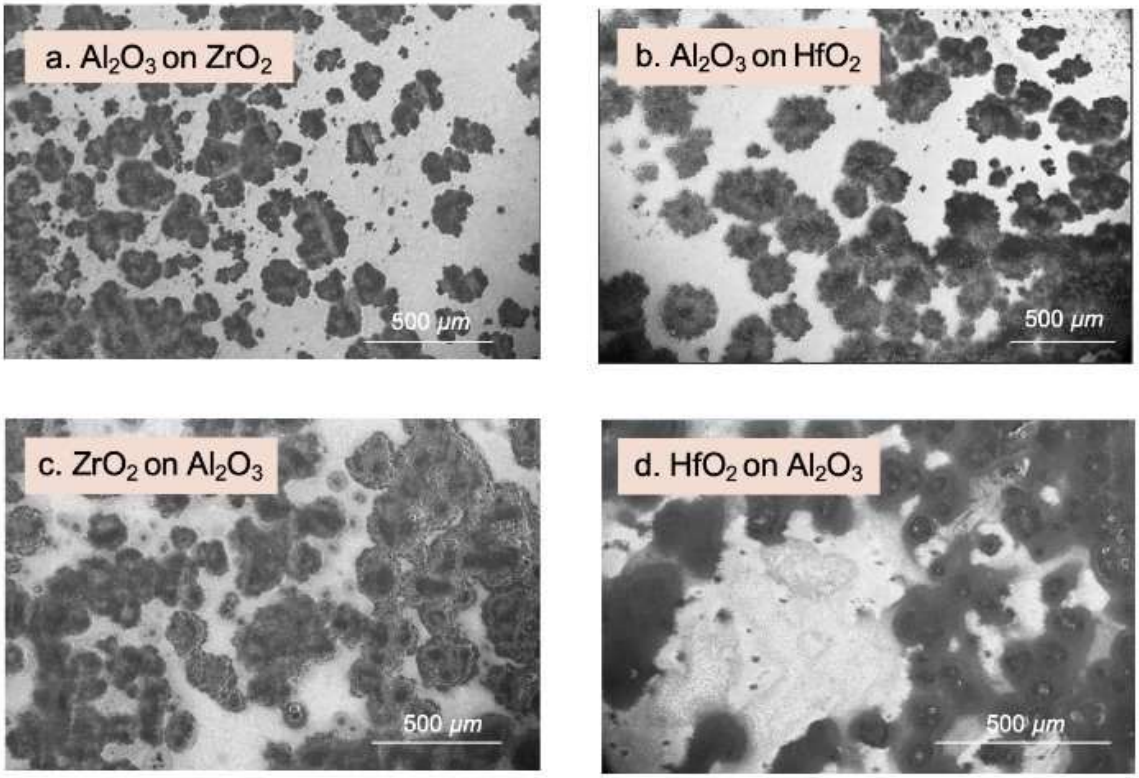

Supplementary Fig. 16. Lithium morphology for a. Al_2O_3 on ZrO_2-Cu b. Al_2O_3 on HfO_2-Cu, c. ZrO_2 on Al_2O_3-Cu, and d. HfO_2 on Al_2O_3-Cu after 1st cycle lithium plating using Li|Cu half-cells with 1 M $LiPF_6$/EC-DEC electrolyte at 1 mA cm^{-2} current density and 0.5 mAh cm^{-2} plating capacity.

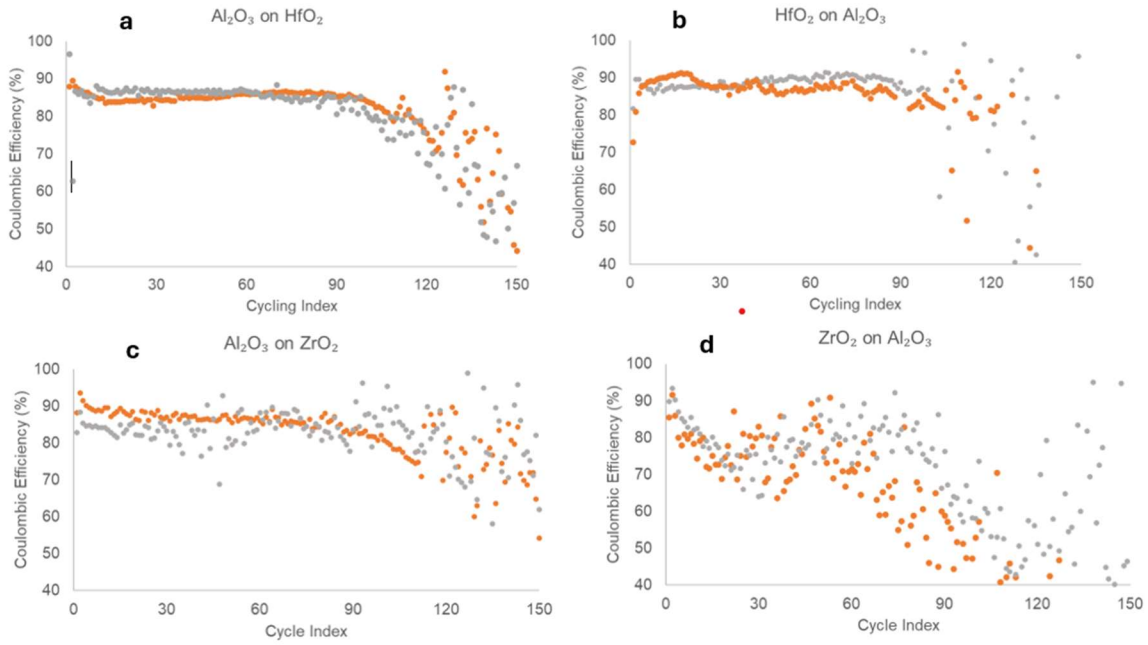

Supplementary Fig. 17. Replicates of long-term cycling performance with Cu modified by a. Al_2O_3 on HfO_2-Cu, b. HfO_2 on Al_2O_3-Cu, c. Al_2O_3 on ZrO_2-Cu, and d. ZrO_2 on Al_2O_3-Cu. Experiments are performed in Li|Cu half-cells using 1 M $LiPF_6$/EC-DEC electrolyte at 1 mA cm^{-2} current density and 1 mAh cm^{-2} plating capacity.

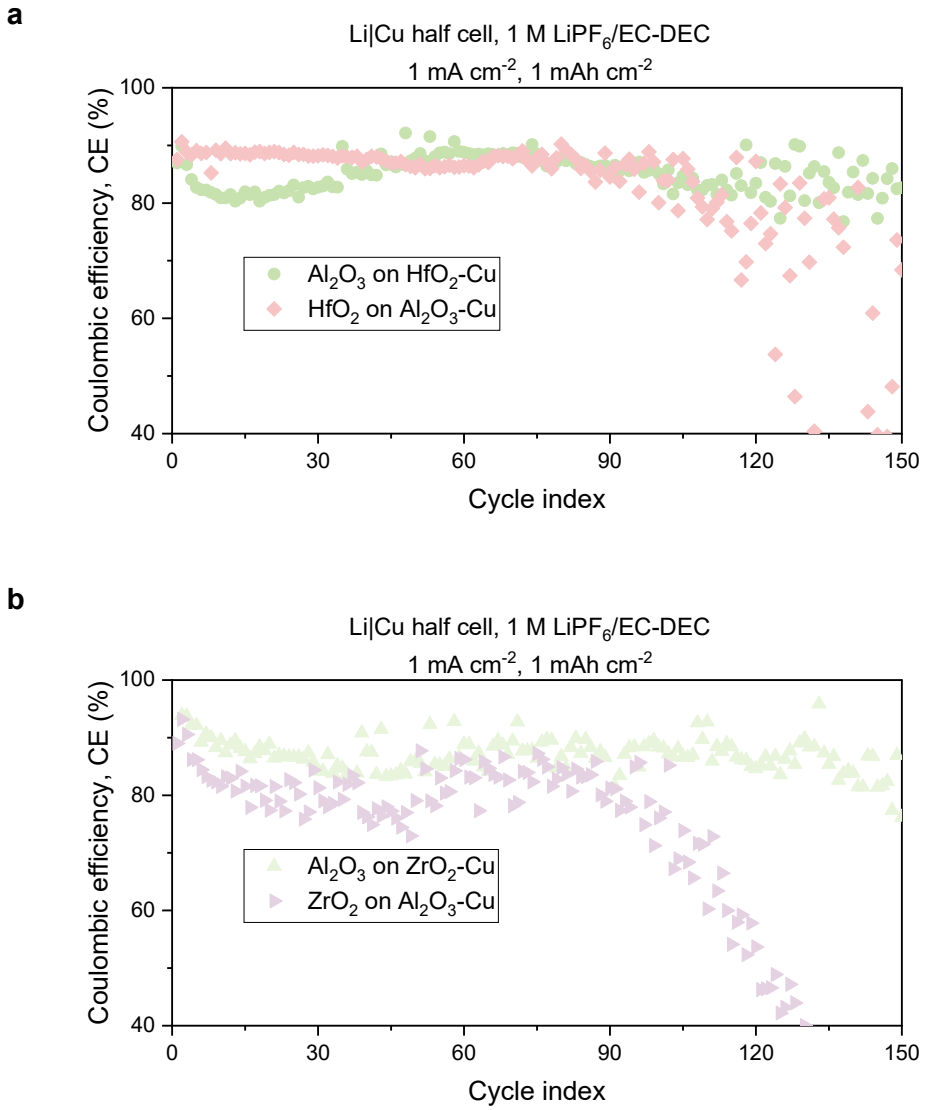

Supplementary Fig. 18. Long-term cycling performance with Cu modified by a. Al_2O_3 on HfO_2-Cu, HfO_2 on Al_2O_3-Cu, b. Al_2O_3 on ZrO_2-Cu, ZrO_2 on Al_2O_3-Cu. Experiments are performed in Li|Cu half-cells using 1 M $LiPF_6$/EC-DEC electrolyte at 1 mA cm^{-2} current density and 1 mAh cm^{-2} plating capacity.

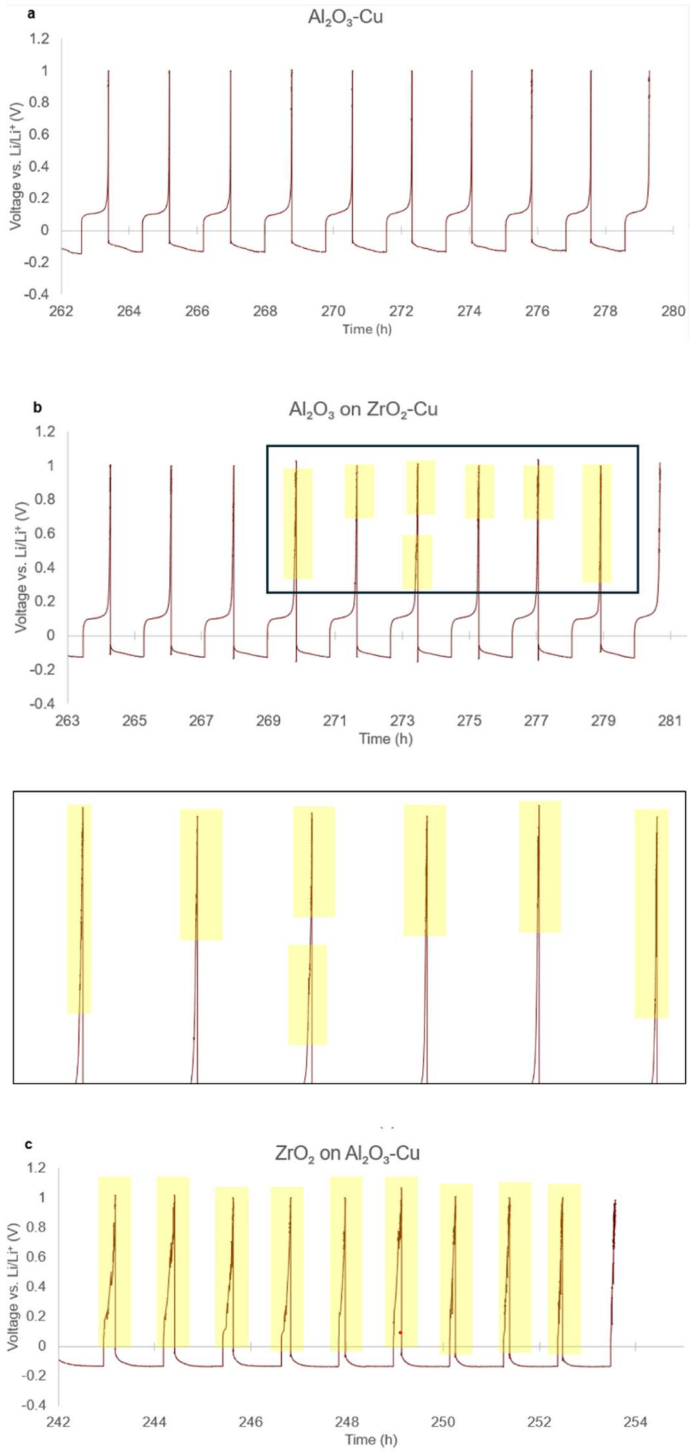

Supplementary Fig. 19. Voltage profiles for Cu modified by a. Al_2O_3-Cu, b. Al_2O_3 on ZrO_2-Cu, and c. ZrO_2 on Al_2O_3-Cu. Experiments are performed in Li|Cu half-cells using 1 M $LiPF_6$/EC-DEC electrolyte at 1 mA cm^{-2} current density and 1 mAh cm^{-2} plating capacity. Highlighted yellow portions indicate areas of instability within the voltage profile.

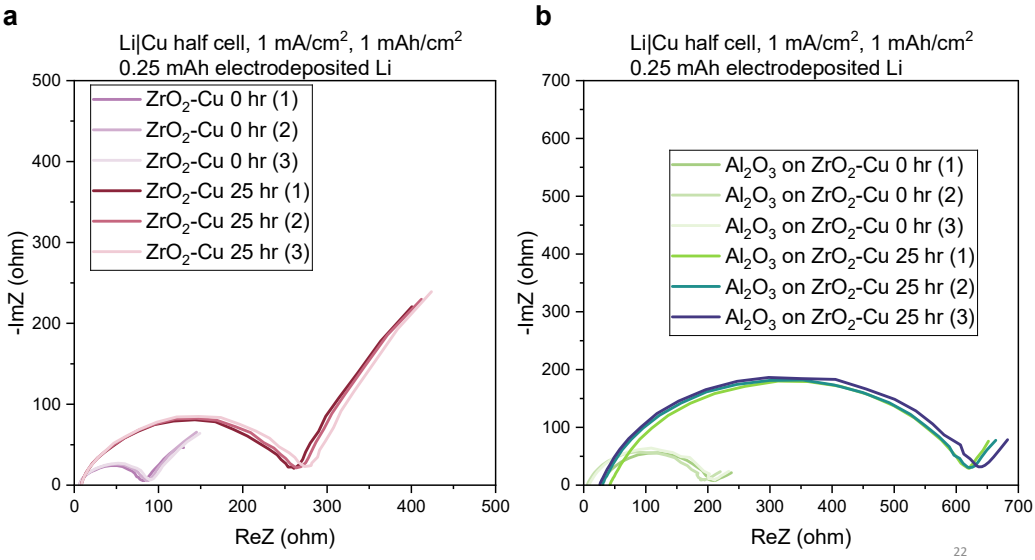

Supplementary Fig. 20. Electrochemical impedance spectroscopy (EIS) of Li|Cu cells with a. ZrO_2 and b. Al_2O_3 on ZrO_2 films to study the relative resistance of the SEI in 1 M $LiPF_6$/EC-DEC electrolyte. The frequency range is 100 mHz to 1 MHz. The initial impedance curve and the change in impedance over 25 hours are shown after Li plating. (1), (2), (3) indicate three replicated measurements.

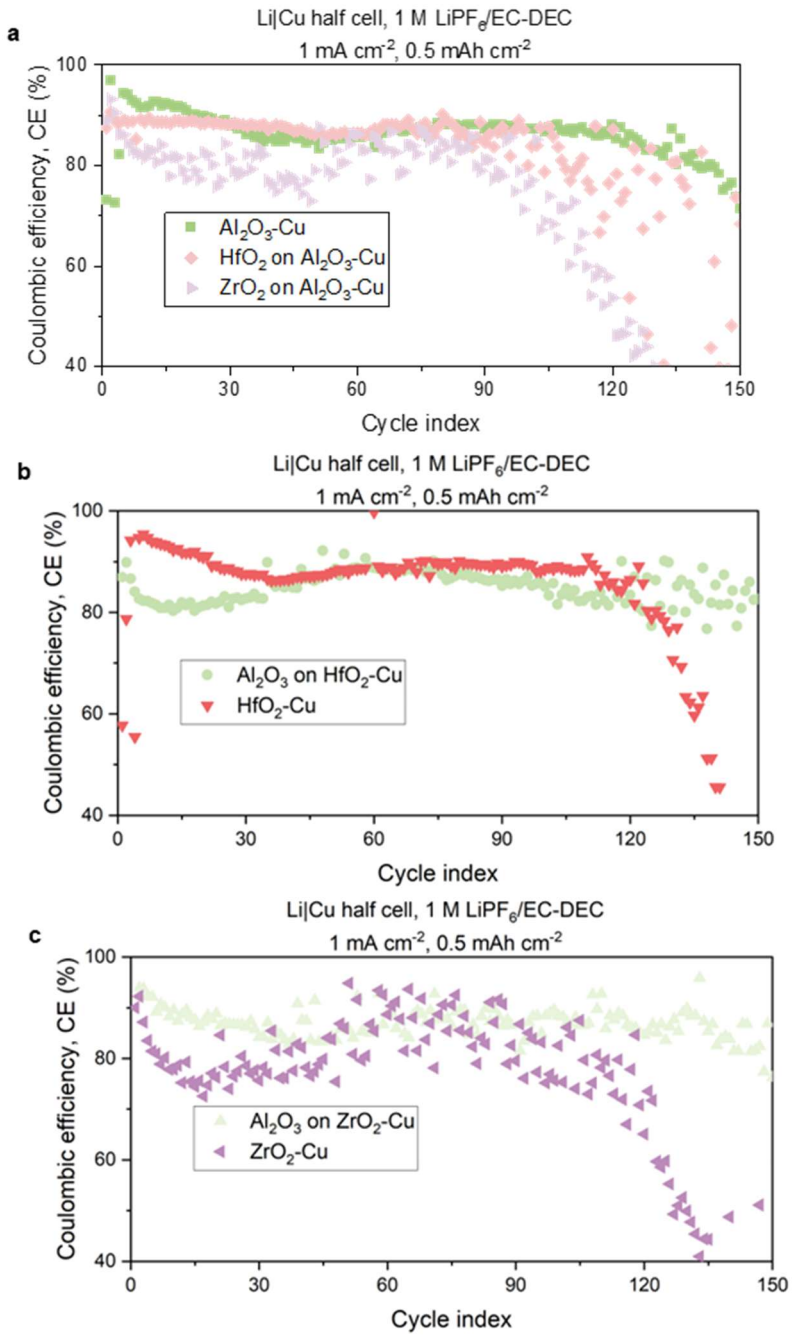

Supplementary Fig. 21. Long-term cycling performance to show impacts of the same Cu/thin film interfaces with Cu modified by a. Al_2O_3-Cu, HfO_2 on Al_2O_3-Cu, and ZrO_2 on Al_2O_3-Cu, b. Al_2O_3 on HfO_2-Cu and HfO_2-Cu, c. Al_2O_3 on ZrO_2-Cu and ZrO_2-Cu. Experiments are performed in Li|Cu half-cells using 1 M $LiPF_6$/EC-DEC electrolyte at 1 mA cm^{-2} current density and 1 mAh cm^{-2} plating capacity.

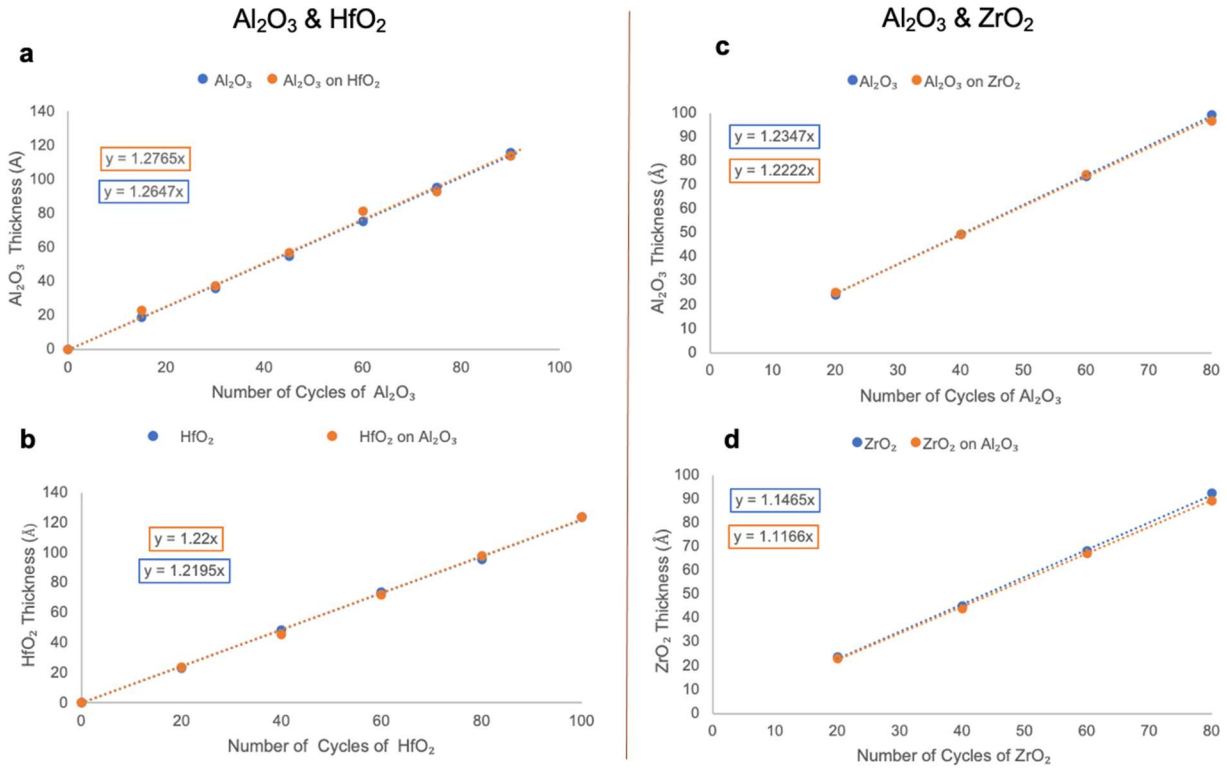

Supplementary Fig. 22. ALD deposition thickness of a. Al_2O_3 on silicon (Si) substrates and HfO_2-modified Si substrates, b. HfO_2 on Si substrates and Al_2O_3-modified Si substrates, c. Al_2O_3 on Si substrates and ZrO_2-modified Si substrates, and d. ZrO_2 on Si substrates and Al_2O_3-modified Si substrates as a function of deposition cycle. Modified Si substrates contain 4 nm Al_2O_3, 6.5 nm HfO_2, and 8.5 nm ZrO_2, respectively, which correspond to half of the thickness used in the 1st cycle nucleation overpotential experiments as described in Fig. 2a and Fig. 4a.